JOURNAL OF SOLID STATE CHEMISTRY **121,** 79–86 (1996)
ARTICLE NO. 0012

Thermal Stability and Structural Changes of $Li_4Mn_5O_{12}$ under Oxygen and Nitrogen Atmosphere

Toshimi Takada,[1] Hiroshi Hayakawa, Toshiya Kumagai, and Etsuo Akiba

Department of Inorganic Materials, National Institute of Materials and Chemical Research, Higashi 1-1, Tsukuba, Ibaraki 305, Japan

Received March 3, 1995; in revised form July 24, 1995; accepted July 31, 1995

The thermal stability and structural changes of well-crystallized $Li_4Mn_5O_{12}$ powder with a grain size of 0.1–0.3 μm have been investigated with thermogravimetric analysis (TGA), X-ray diffraction (XRD), and high-temperature X-ray diffraction measurements (HT-XRD). $Li_4Mn_5O_{12}$ crystallites are stable at temperatures up to 600°C in oxygen or air, but decompose to spinel $LiMn_2O_4$ and monoclinic Li_2MnO_3 at temperatures between 530 and 680°C, and to $LiMnO_2$ and Mn_3O_4 at temperatures above 680°C in nitrogen. No apparent structural change was detected with XRD and HT-XRD when $Li_4Mn_5O_{12}$ was heated in O_2 up to 700°C, but a reversible weight loss/gain due to the evolution/uptake of oxygen was observed by TGA between 400–700°C. The deficiency of oxygen in $Li_4Mn_5O_{12-\delta}$ is found to be in the region $0 < \delta \leq 0.5$.

1. INTRODUCTION

Lithium manganese oxides are of interest as lithium insertion electrodes for rechargeable lithium batteries because they offer high cell voltage, wide operating temperature, and long shelf life with much lower cost as compared to $LiNiO_2$ and $LiCoO_2$. Particular attention has been focused on the spinel $LiMn_2O_4$ (1–4) in which the $[Mn_2]O_4$ framework provides a three-dimensional interstitial space for Li^+ ion transport. It has been found that the cubic symmetry of spinel structure is maintained over a wide composition range of $Li_x[Mn_2]O_4$ ($0 \leq x \leq 1$) which allows the electrode to expand and contract isotropically during lithium insertion/extraction reactions. The recent work of Thackeray's group (1, 5, 6) demonstrated that excellent capacity retention on cycling was obtained from Mn^{4+} defect spinels $Li/Li_4Mn_5O_{12}$ and $Li/Li_2Mn_4O_9$.

The research directed toward the improvement of capacity retention in rechargeable lithium/spinel lithium manganese oxides cells has covered much ground: (i) Optimization of electrolyte composition (7, 8), spinel electrode composition $Li_xMn_{2-\delta}O_4$ (9), and manganese substitution $Li_xM_yMn_{2-y}O_4$ (M = Ti, Ge, Fe, Zn, Ni, Mg, etc.) (4, 10). (ii) Development of the low-temperature synthesis process (11, 12), whose products possess smaller grain size, higher capacity, and longer cycle life as compared to those products obtained with the high temperature needed for solid state reactions. Recently, Tarascon and co-workers (13) have demonstrated how sensitive the oxygen stoichiometry and therefore, the electrochemical properties of lithium intercalation within spinel $Li_xMn_2O_{4+\delta}$ are to changes in the synthesis conditions for $LiMn_2O_4$ powder, such as synthesis and annealing temperatures and cooling rates. Studies on Mn^{4+} defect spinels $Li_2O \cdot yMnO_2$ (y = 2.5–4) with end members of $Li_4Mn_5O_{12}$ (y = 2.5) and $Li_2Mn_4O_9$ (y = 4) are, however, limited to those poorly crystalline powders obtained from the solid state reaction of Li_2CO_3 or LiOH, and $MnCO_3$ or MnO_2 at temperatures below 400°C, because the concomitant formation of Mn^{3+} occurs by the reduction of Mn^{4+} when the reaction temperature is raised above 400°C (14, 15). Recently, we reported that well-crystallized $Li_4Mn_5O_{12}$ can be prepared at a temperature up to 700°C from a eutectic mixture by using lithium acetate LiOAc and manganese nitrate $Mn(NO_3)_2$ as starting materials (16). The structure of $Li_4Mn_5O_{12}$ crystallites was refined by the Rietveld method from powder X-ray diffraction data as a cubic spinel, a = 8.1616(5) Å, space group $Fd\bar{3}m$. Our preliminary TGA results showed that $Li_4Mn_5O_{12}$ crystallites possess different thermal stability upon the heating atmosphere.

In this work, we have systematically investigated the thermal stability and structural changes of $Li_4Mn_5O_{12}$ using thermogravimetric analysis, X-ray diffraction, and high-temperature X-ray diffraction. High resolution scanning electron micrographs are presented to show the morphology of the $Li_4Mn_5O_{12}$ crystallites. Details of the decomposition process of $Li_4Mn_5O_{12}$ under oxygen, air, and nitrogen are discussed in comparison with that of $LiMn_2O_4$.

2. EXPERIMENTAL

Synthesis of $Li_4Mn_5O_{12}$. LiOAc·$2H_2O$ and $Mn(NO_3)_2 \cdot 6H_2O$, 99.9% pure (from WAKO Pure Chemical Indus-

[1] To whom correspondence should be addressed.

0022-4596/96 $12.00

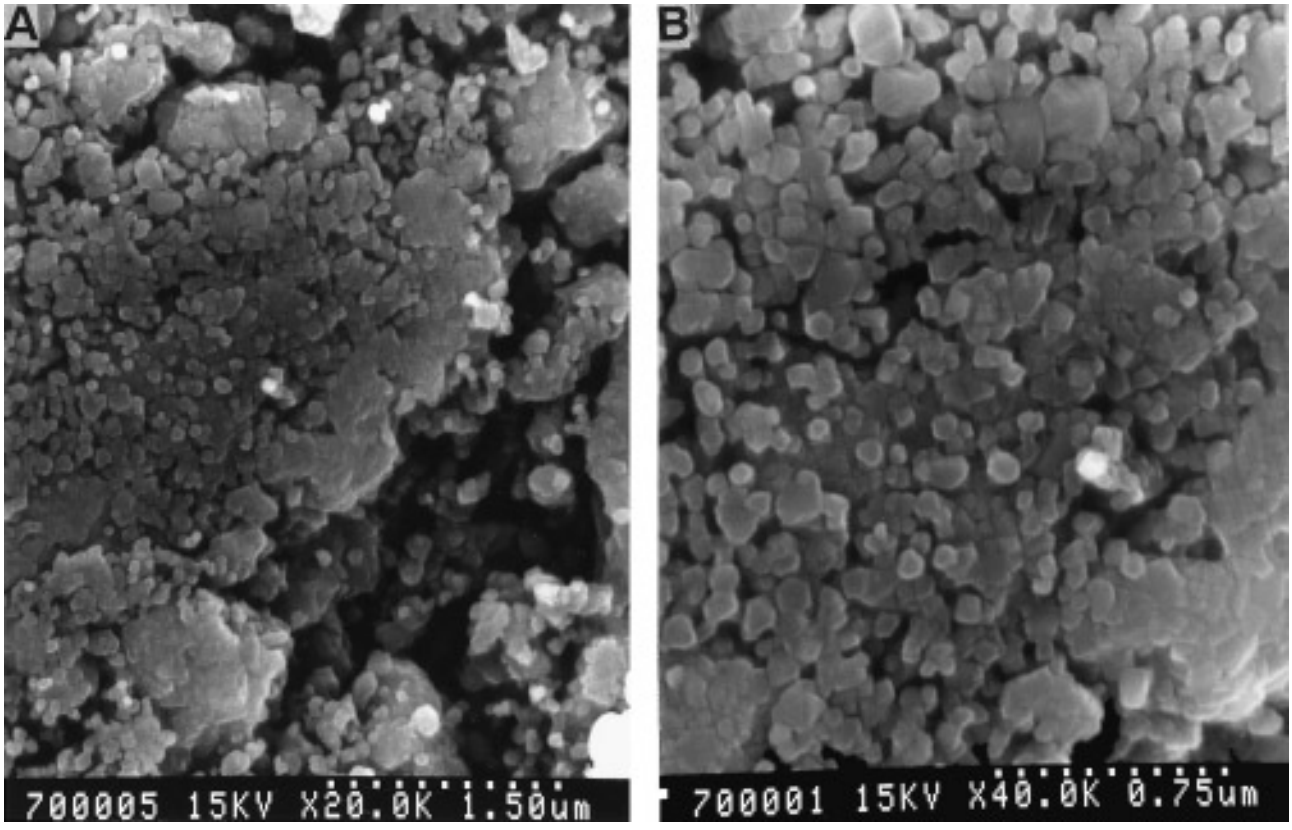

FIG. 1. Scanning electron micrographs of the $Li_4Mn_5O_{12}$ crystallites obtained at 700°C. (sample ANT700-3D); B is the enlargement of A.

tries, Ltd.), were used as starting materials. A stoichiometric amount of the raw materials was first heated at 100°C to obtain a uniform eutectic solution and then slowly oxidized at 200°C with flowing O_2, thereby converting the eutectic solution to a solid Li–Mn–O precursor. Powder sample (ANT700-1D) was obtained by heating the ground precursor first at 500°C for 1 day and then at 700°C for another day. The well-sintered sample (ANT700-3D) was prepared by heating the pelletized precursor (5-mm-thick, 10 mm in diameter) at 500°C for 1 day and thereafter at 700°C for 3 days. All samples were heated at a rate of 100°C/hr and slowly cooled to room temperature in the furnace (about 7 hr) with 200 ml/min flowing O_2. Details of the preparation process are described in our previous report (16).

The standard spinel $LiMn_2O_4$ was prepared in air by the solid reaction of Mn_2O_3 and Li_2CO_3 in a 2:1 molar ratio. The mixture was heated first at 650°C for 12 hr in order to decompose the Li_2CO_3 and then at 850°C for 24 hr. The monoclinic phase Li_2MnO_3 was prepared by the solid reaction in air of Li_2CO_3 and $MnCO_3$ in a 1:1 molar ratio at 800°C for 24 hr.

Electron microscopy. Scanning electron micrographs (SEM) were taken at room temperature on a Hitachi S-800 microscope equipped with a field emission gun, at 15 kV. The specimen was coated with about 10-nm-thick Pt for observation.

Thermal analysis. TGA curves were measured using a Seiko SSC5020 thermal analyzer system at a heating/cooling rate of 10°C/min with 200 ml/min flow of O_2 or N_2. About 30 mg of the powder sample or lumps of the well-sintered sample were used as specimens and 99.99% pure α-Al_2O_3 powder was used as the standard material.

X-ray diffraction. Powder X-ray diffraction patterns were collected at room temperature on a Rigaku RAX-I X-ray diffractometer with Cu$K\alpha$ radiation monochromated by a graphite single crystal at 40 kV, 30 mA. High temperature X-ray diffraction patterns were collected on a MAC-MXP^3 Automatic X-Ray diffractometer at 40 kV, 30 mA, from room temperature to 1005°C at a heating rate of 10°C/min with 100 ml/min flow of air or N_2. The sample was pelletized (10 × 7 mm, 1-mm-thick) and mounted on a Pt holder.

3. RESULTS AND DISCUSSION

3.1. Morphology of Well-Crystallized $Li_4Mn_5O_{12}$

Figure 1 shows a typical SEM image of the $Li_4Mn_5O_{12}$ crystallites prepared at 700°C (sample ANT700-3D). Mi-

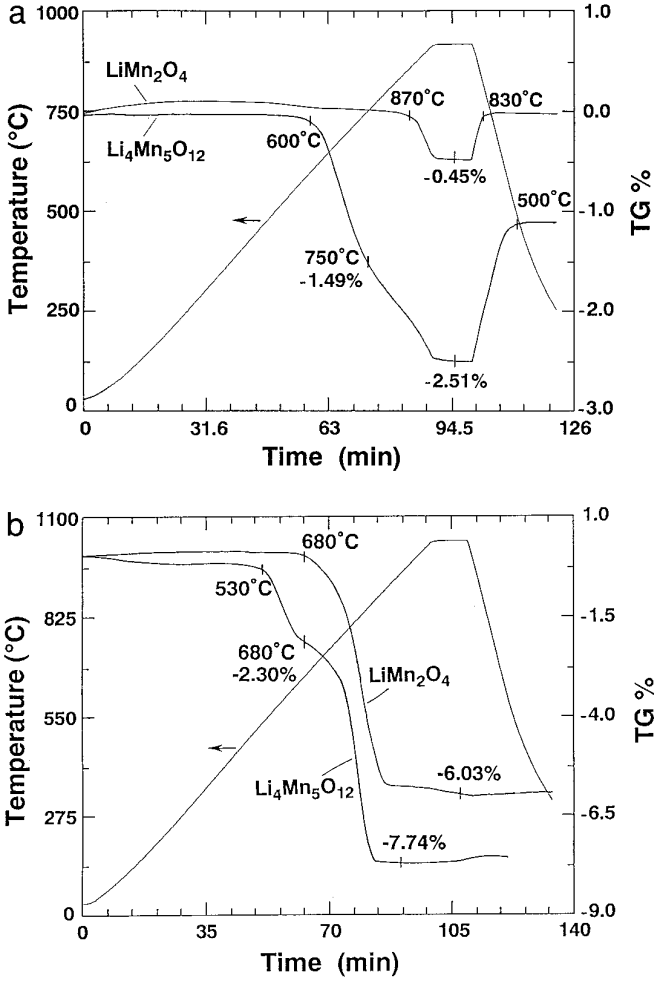

FIG. 2. TGA curves of $Li_4Mn_5O_{12}$ measured with 200 ml/min flow of (a) O_2 and (b) N_2, together with that of $LiMn_2O_4$.

crograph B is the enlargement of A. Clearly, the size of $Li_4Mn_5O_{12}$ crystallites in the sample was uniformly distributed between 0.1 and 0.3 μm. The uniformity in the size and shape of the crystallites as shown by micrographs A and B could be a result of the homogeneity of the Li–Mn–O precursor.

3.2. Thermal Stability and Structural Changes of $Li_4Mn_5O_{12}$ up to 930°C

Figure 2a shows the TGA curve of sample ANT700-1D with flowing O_2, along with that of the standard $LiMn_2O_4$. The specimen was first heated up to 930°C at a rate of 10°C/min and then cooled to room temperature at a rate of 40°C/min after holding the temperature at 930°C for 10 min. $Li_4Mn_5O_{12}$ was fairly stable at temperatures up to 600°C, but thereafter the first weight loss of 1.49% was observed between 600 and 750°C; the second weight loss proceeded to 930°C. The sample recovered its weight by 1.48% during cooling from 930 to 500°C. On the whole, the maximum reversible weight loss/gain was about 1.5% for the $Li_4Mn_5O_{12}$ sample. A completely reversible weight loss/gain of 0.45% was observed for $LiMn_2O_4$ between 870 → 930°C and 930 → 830°C, which corresponds to an evolution/uptake of 0.025 O_2 for each $LiMn_2O_4$, i.e., $LiMn^{3+}\,Mn^{4+}O_4 \Leftrightarrow LiMn^{3+}{}_{1.1}Mn^{4+}{}_{0.9}O_{3.95} + 0.025\ O_2$. It should be noted that the standard $LiMn_2O_4$ was prepared at 850°C. See Section 3.3 and Ref. (13) by Tarascon and co-workers for details about this reversible weight loss/gain. In addition, the TGA curve for the $Li_4Mn_5O_{12}$ sample measured with 100 ml/min flowing air is the same as that measured with flowing O_2, thus the results obtained under O_2 discussed below are applicable to the ordinary air atmosphere.

A significant effect of heating atmosphere on the stability of $Li_4Mn_5O_{12}$ was observed. Figure 2b shows the TGA curves measured with flowing N_2 under the same condition as in Fig. 2a. For the $Li_4Mn_5O_{12}$ sample, two weight loss steps were observed in the temperature ranges of 530–680°C and 680–870°C. For the standard $LiMn_2O_4$ sample, only one step weight loss of about 6% was observed between 680 and 900°C. No weight recovery was detected for both $Li_4Mn_5O_{12}$ and $LiMn_2O_4$ samples during the whole cooling process from 930°C to room temperature.

The effects of heating atmosphere on the structural change of $Li_4Mn_5O_{12}$ were observed in the *in situ* high temperature X-ray diffraction measurements. Figure 3a shows the HT-XRD patterns of sample ANT700-1D collected at 400, 600, 700, 805, 845, 905, 945, and 1005°C with 100 ml/min flow of air. Air was used instead of pure oxygen due to the limitation from the shielding assembly. No apparent structural change was detected at temperatures below 600°C. The precipitation of Li_2MnO_3 can be slightly seen at 700°C and is more apparent at 805 and 845°C. Only the diffraction peaks from Li_2MnO_3 were detected at 945°C and above; on the other hand, only the XRD pattern of $LiMn_2O_4$ was detected on the backside (the surface adhered to the Pt holder) of the specimen after the HT-XRD measurements. Considering the fact that the HT-XRD data reflect information mainly about the surface layer of the specimen where Li_2MnO_3 has a strong tendency to form under our HT-XRD configuration, the peaks of Li_2MnO_3 could be intensified compared to those in the ordinary powder XRD patterns; besides, the $Li_4Mn_5O_{12}$ sample was prepared at 700°C and the peaks of Li_2MnO_3 at 700°C are rather small, so it can be concluded that the formation of Li_2MnO_3 as an indication of the decomposition of $Li_4Mn_5O_{12}$ occurs at temperatures higher than 700°C in air. Figure 3b shows the HT-XRD patterns of sample ANT700-1D collected with flowing N_2 from room temperature (RT) to 900°C. Obviously, no structural change was detected under 500°C. The peaks of the second-

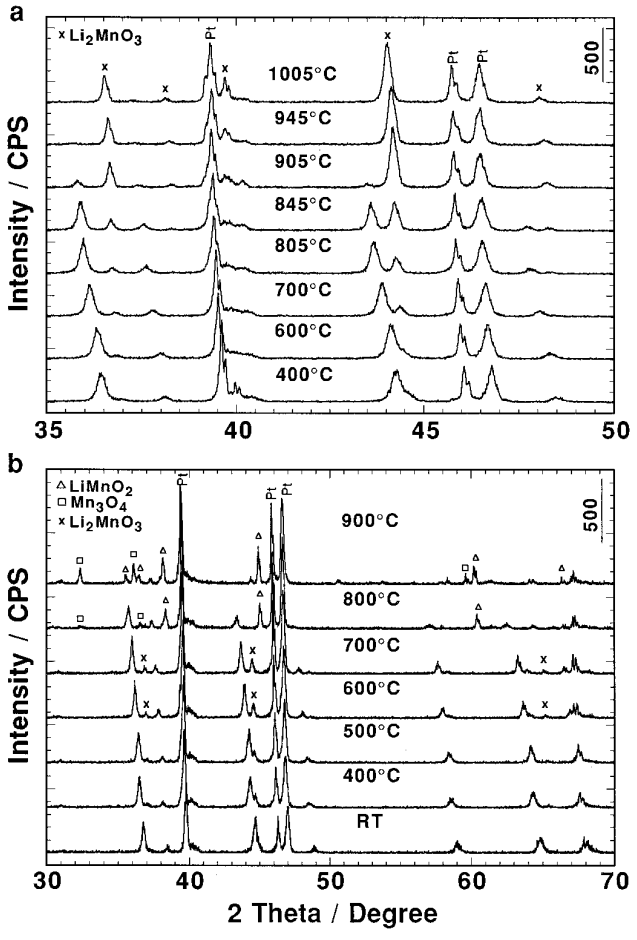

FIG. 3. High-temperature X-ray diffraction patterns of $Li_4Mn_5O_{12}$ collected at various temperatures, with 100 ml/min flow of (a) air and (b) N_2.

phase Li_2MnO_3 appeared at 600 and 700°C but disappeared at 800 and 900°C, instead, the diffraction peaks of $LiMnO_2$ and Mn_3O_4 were detected at 800 and 900°C.

By combining the results of HT-XRD with the corresponding TGA curves, we conclude that $Li_4Mn_5O_{12}$ possesses different thermal stability under oxygen, inert, or reductive atmospheres. In O_2, the decomposition of $Li_4Mn_5O_{12}$ to $LiMn_2O_4$ and Li_2MnO_3 occurs at temperatures above 750°C, which corresponds to a weight loss of 3.24% due to the evolution of O_2 according to

$$Li_4Mn_5O_{12} \xrightarrow[\geq 750°C \text{ in } O_2]{-3.24\ wt\%} 2\,LiMn_2O_4 + Li_2MnO_3 + \frac{1}{2}O_2 \uparrow . \quad [1]$$

No further decomposition was detected up to 1005°C. The reversible weight loss/gain will be discussed in Section 3.3. Whereas, in N_2, the decomposition of $Li_4Mn_5O_{12}$ to $LiMn_2O_4$ and Li_2MnO_3 starts at 530°C, which is much lower than 750°C, further decomposition to $LiMnO_2$ and Mn_3O_4 proceeds at temperatures above 680°C, which will lead to another weight loss of 5.39% on the basis of

$$2\,LiMn_2O_4 + Li_2MnO_3 \xrightarrow[>680°C \text{ in } N_2]{-5.39\ wt\%} 4\,LiMnO_2 + \frac{1}{3}Mn_3O_4 + \frac{5}{6}O_2 \uparrow . \quad [2]$$

A total weight loss of 8.63% is calculated based on Eq. [3] in the case that $Li_4Mn_5O_{12}$ directly decomposes to $LiMnO_2$ and Mn_3O_4.

$$Li_4Mn_5O_{12} \xrightarrow[>680°C \text{ in } N_2]{-8.63\ wt\%} 4\,LiMnO_2 + \frac{1}{3}Mn_3O_4 + \frac{4}{3}O_2 \uparrow \quad [3]$$

Similarly, the decomposition of standard spinel $LiMn_2O_4$ to $LiMnO_2$ and Mn_3O_4, which occurs directly at temperatures above 680°C in N_2, will correspond to a weight loss of 5.90% according to

$$LiMn_2O_4 \xrightarrow[>680°C \text{ in } N_2]{-5.90\ wt\%} LiMnO_2 + \frac{1}{3}Mn_3O_4 + \frac{1}{3}O_2 \uparrow . \quad [4]$$

This weight loss is in good agreement with the TGA detected 6% within the experimental error. Since Li_2MnO_3 is fairly stable up to 930°C and the decomposition of $LiMn_2O_4$ occurs at temperatures above 680°C in N_2, it is more reasonable to explain the observed two-step weight loss for $Li_4Mn_5O_{12}$ sample as: the first weight loss is due to the decomposition of $Li_4Mn_5O_{12}$ to $LiMn_2O_4$ and Li_2MnO_3 (Eq. [1]), while the second one proceeds via the decomposition of $LiMn_2O_4$ (Eq. [4]). This process corresponds to a total weight loss of 7.55% that is consistent with the detected 7.7%. These complex decomposition process will be further discussed in Section 3.4.

3.3. Thermal Stability and Structural Changes of $Li_4Mn_5O_{12}$ below 750°C

Detailed measurements of TGA between RT and 700°C and powder X-ray diffraction of $Li_4Mn_5O_{12}$ samples treated under corresponding conditions were conducted to make it clear what happens with the reversible weight loss/gain in O_2, and to further verify the decomposition

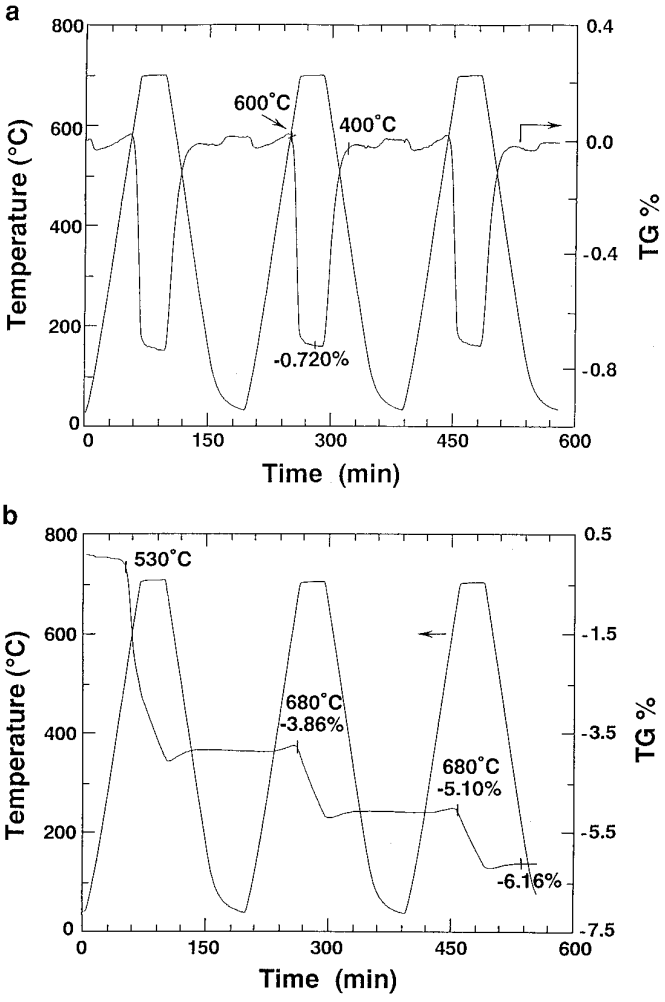

FIG. 4. TGA curves of $Li_4Mn_5O_{12}$ as the sample was repeatedly heated/cooled between RT and 700°C, with 200 ml/min flow of (a) O_2 and (b) N_2.

reactions of $Li_4Mn_5O_{12}$ in N_2. Figure 4 shows the TGA curves of sample ANT700-3D with 200 ml/min of flowing (a) O_2, and (b) N_2. The specimen was treated three times at a heating/cooling rate of 10°C/min between RT and 700°C, following a three-step heat-treatment cycle: heating up to 700°C, holding there for 30 min, and then cooling to RT. In O_2, a weight loss of 0.72% was detected when the sample was heated from 600 to 700°C, and the sample recovered its lost weight upon cooling from 700 to 400°C. Figure 4a clearly shows that the reversible weight loss/gain repeated with the cycling of heating/cooling process. No decline in the reversible weight loss/gain was observed even after 8 cycles. In N_2, once again, no weight recovery was detected during the cooling process. Clearly, the first step decomposition of $Li_4Mn_5O_{12}$ to $LiMn_2O_4$ and Li_2MnO_3, corresponding to 3.24% weight loss, started at 530°C and was completed within the first heating cycle. The second decomposition step, which corresponds to another weight loss of 5.39% based on Eq. [2], was limited by the kinetics and proceeded rather slowly throughout the three heating cycles when temperature was raised above 680°C.

Figure 5a shows the room temperature powder X-ray diffraction patterns for sample ANT700-1D after repeated heating from RT to 700°C for 3–8 times with flowing O_2. For comparison, that for the ANT700-1D sample before the re-treatments is presented as $Li_4Mn_5O_{12}$. It is evident that the framework of $Li_4Mn_5O_{12}$ remained intact after these retreatments. However, the structure of the sample reheated in N_2 changed notably, as detected by the changes in the diffraction patterns (Fig. 5b). The diffraction peaks for the sample reheated at 580°C for 1 day (Re-580°C-1D) were assigned to the reflections from both $LiMn_2O_4$ and Li_2MnO_3, which verifies the decomposition of $Li_4Mn_5O_{12}$ to $LiMn_2O_4$ and Li_2MnO_3 in the temperature range 530–

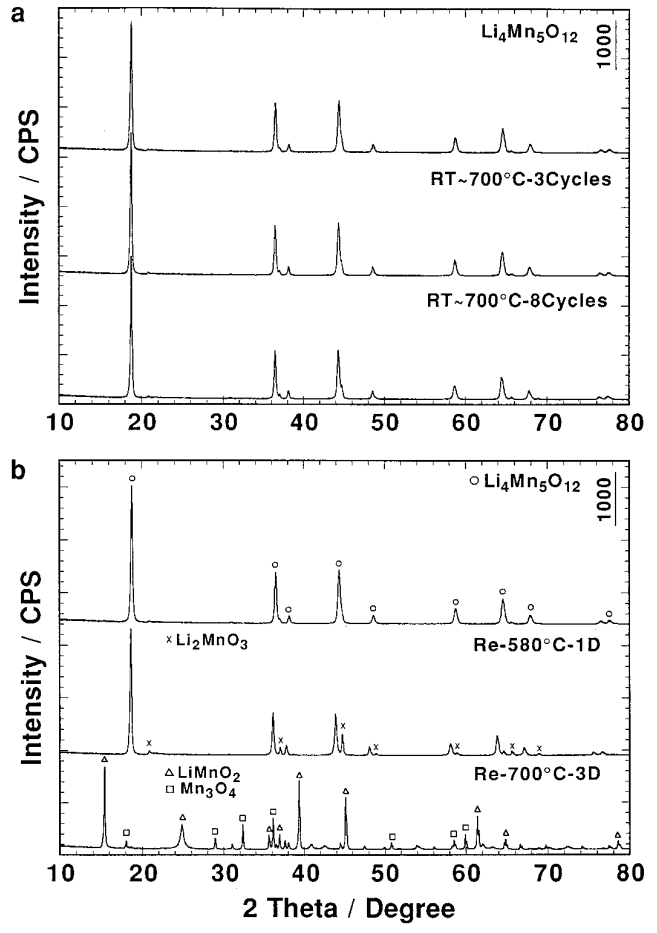

FIG. 5. Room-temperature powder X-ray diffraction patterns of the reheated $Li_4Mn_5O_{12}$ samples, together with that of the original $Li_4Mn_5O_{12}$: (a) repeated heating/cooling between RT and 700°C, 3 and 8 times with flowing O_2; (b) reheating with flowing N_2 at 580°C for 1 day and at 700°C for 3 days.

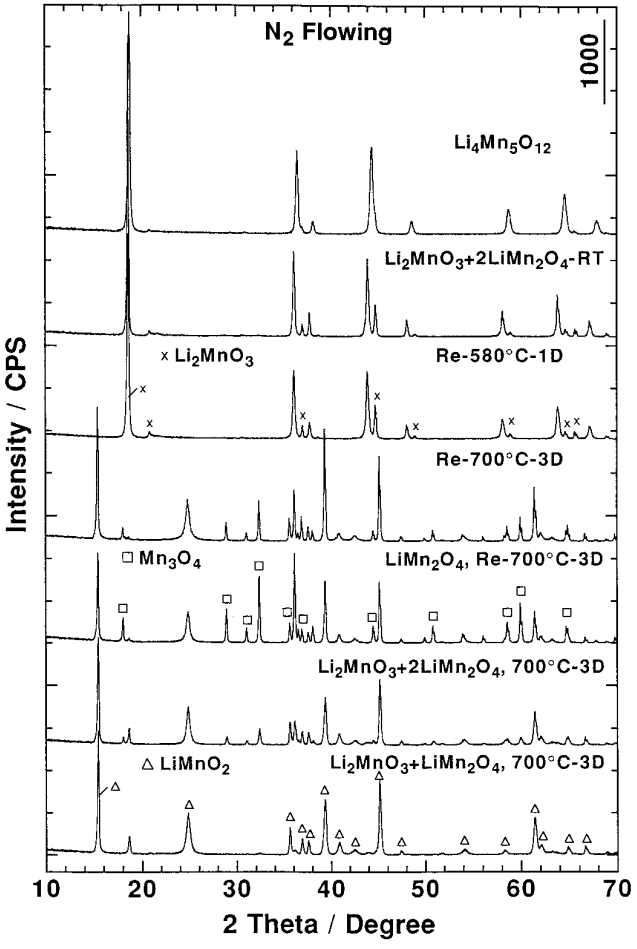

FIG. 6. Room temperature powder X-ray diffraction patterns of the reheated $LiMn_2O_4$, the $Li_4Mn_5O_{12}$ samples, and the reaction products of $LiMn_2O_4$ and Li_2MnO_3 at 700°C for 3 days with flowing N_2, along with those of the original $Li_4Mn_5O_{12}$ and the mixture of $2LiMn_2O_4 + Li_2MnO_3$ at room temperature.

680°C. Principal diffraction peaks of both $LiMnO_2$ and Mn_3O_4 were detected for the sample reheated at 700°C for 3 days (Re-700°C-3D), which indicates the presence of $LiMnO_2$ and Mn_3O_4 in the decomposed $Li_4Mn_5O_{12}$ sample at temperatures above 680°C in N_2.

From the results mentioned above, we conclude that the reversible weight loss/gain observed below 750°C with flowing O_2/air for $Li_4Mn_5O_{12}$ samples occurs without destroying the spinel framework. By assuming that this weight loss/gain results from the evolution/uptake of oxygen due to the reduction/oxidation between $Mn^{4+} \leftrightarrow Mn^{3+}$,

$$Li_4Mn_5^{4+}O_{12} \underset{\text{Cooling}}{\overset{\text{Heating}}{\rightleftharpoons}} Li_4Mn_x^{3+}Mn_{(5-x)}^{4+}O_{(12-(x/2))} + \frac{x}{4}O_2(g), \quad [5]$$

it is calculated that the 0.72% weight loss from 600 to 700°C (Fig. 4a) leads to the evolution of 0.11 O_2 from one $Li_4Mn_5O_{12}$, accompanied by the reduction of 8.9% Mn^{4+} to Mn^{3+}. Upon cooling from 700 to 400°C, about 0.11 O_2 is absorbed from the atmosphere, i.e., $Li_4Mn_5^{4+}O_{12} \leftrightarrow Li_4Mn_{0.44}^{3+}Mn_{4.56}^{4+}O_{11.78} + 0.11\ O_2$. Similarly, the weight loss of 1.5% (Fig. 2a) when the sample was heated to 750°C should correspond to an evolution of 0.23 O_2 from each $Li_4Mn_5O_{12}$ with reduction of 18.4% Mn^{4+} to Mn^{3+}, i.e., $Li_4Mn_5^{4+}O_{12} \leftrightarrow Li_4Mn_{0.92}^{3+}Mn_{4.08}^{4+}O_{11.54} + 0.23\ O_2$.

Consequently, the maximum of the reversible reduction/oxidation $Mn^{4+} \leftrightarrow Mn^{3+}$ under oxygen atmosphere without destroying the spinel framework is approximately estimated to be 20% of the Mn within each $Li_4Mn_5O_{12}$. Samples with deficiency of oxygen at temperatures above 400°C can be presented as $Li_4Mn_5O_{12-\delta}$ with $0 < \delta \leq 0.5$ or between the end members of $Li_4Mn_5^{4+}O_{12}$ and $Li_4Mn^{3+}Mn_4^{4+}O_{11.50}$. Also, samples synthesized under different conditions could be slightly deficient in oxygen, but with $0 < \delta \ll 0.5$ in $Li_4Mn_5O_{12-\delta}$ when the sample is slowly cooled/annealed in an oxygen atmosphere.

3.4. Verification of the Decomposition of $Li_4Mn_5O_{12}$ under Flowing N_2

In order to clarify the decomposition process of $Li_4Mn_5O_{12}$ in N_2, the decomposition of $LiMn_2O_4$ and the reaction of $LiMn_2O_4$ and Li_2MnO_3 were investigated under flowing N_2. Theoretically, reactions between $LiMn_2O_4$ and Li_2MnO_3, Eqs. [6] and [7], are expected for the cases that are mixed in a molar ratio of 2:1 and 1:1, respectively.

$$2\,LiMn_2O_4 + Li_2MnO_3 \xrightarrow[>680°C\text{ in }N_2]{-5.57\text{ wt\%}} 4\,LiMnO_2 + \frac{1}{3}Mn_3O_4 + \frac{5}{6}O_2 \uparrow \quad [6]$$

$$LiMn_2O_4 + Li_2MnO_3 \xrightarrow[>680°C\text{ in }N_2]{-5.37\text{ wt\%}} 3\,LiMnO_2 + \frac{1}{2}O_2 \uparrow \quad [7]$$

TGA curves collected under the same conditions for the mixtures of $LiMn_2O_4$ and Li_2MnO_3 are very similar to that of $LiMn_2O_4$ (Fig. 2b). Only one step weight loss of 5.6% for the 2:1 mixture, and 5.4% for the 1:1 mixture, were observed between 680 and 880°C, which are in good agreement with the expected reactions Eqs. [6] and [7], respectively.

Figure 6 shows the powder X-ray diffraction patterns for the samples including: the original $Li_4Mn_5O_{12}$ (ANT700-1D) and the mixture of $LiMn_2O_4$ and Li_2MnO_3

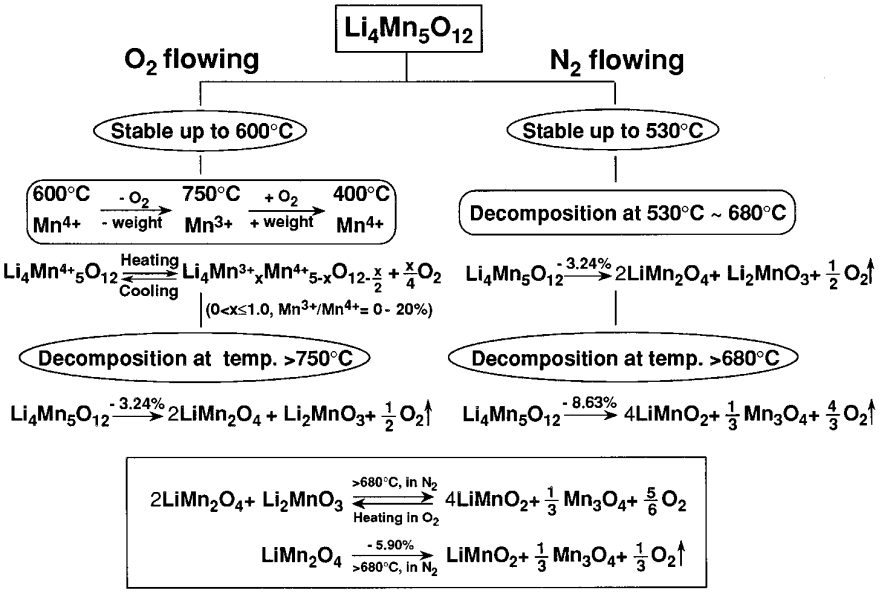

FIG. 7. The thermal stability and decomposition reactions of $Li_4Mn_5O_{12}$ under flowing O_2 and N_2.

(2:1, at room temperature); the re-heated $LiMn_2O_4$ and $Li_4Mn_5O_{12}$ samples; and the products of the reactions between $LiMn_2O_4$ and Li_2MnO_3 under flowing N_2. Clearly, the $Li_4Mn_5O_{12}$ sample reheated at 580°C (Re-580°C-1D) gave the same XRD pattern as that of the original mixture $2LiMn_2O_4 + Li_2MnO_3$-RT, which once more verifies the decomposition of $Li_4Mn_5O_{12}$ to $2LiMn_2O_4 + Li_2MnO_3$ at temperatures between 530 and 680°C. The XRD pattern of both the reheated $Li_4Mn_5O_{12}$ sample (Re-700°C-3D) and $LiMn_2O_4$ ($LiMn_2O_4$, Re-700°C-3D) is very similar to that of the products of reaction Eq. [6] reacted at 700°C for 3 days. ($2LiMn_2O_4+Li_2MnO_3$, 700°C-3D). All diffraction peaks for these three samples were assigned to those from $LiMnO_2$ and Mn_3O_4 as theoretically expected from Eqs. [4] and [6]. As expected from Eq. [7], $LiMnO_2$ was the sole product detected by XRD for the 1:1 mixture of $LiMn_2O_4$ and Li_2MnO_3 after reacted at 700°C for 3 days under flowing N_2 ($LiMn_2O_4 + Li_2MnO_3$, 700°C-3D).

Consequently, the decomposition of $Li_4Mn_5O_{12}$ at temperatures above 680°C gives the same final products consisting of $LiMnO_2$ and Mn_3O_4, whether it directly decomposes to $LiMnO_2$ and Mn_3O_4 via reaction Eq. [3] or proceeds via an intermediate phase consisting of $2LiMn_2O_4 + Li_2MnO_3$ through Eq. [2]. The reaction $2LiMn_2O_4 + Li_2MnO_3$ (Eq. [6]), which occurs at temperatures above 680°C in N_2, generates the same products $LiMnO_2$ and Mn_3O_4. As a result, Li_2MnO_3 does not remain in the decomposed $Li_4Mn_5O_{12}$ sample reheated at temperatures above 680°C in N_2. In addition, it is important to mention that the reactions between $LiMn_2O_4$ and Li_2MnO_3 are reversible depending on the heating temperature and atmosphere.

$$2\ LiMn_2O_4 + Li_2MnO_3 \underset{\text{heating in } O_2}{\overset{>680^\circ C \text{ in } N_2}{\rightleftharpoons}} 4\ LiMnO_2 + \frac{1}{3}Mn_3O_4 + \frac{5}{6}O_2 \quad [6]$$

$$LiMn_2O_4 + Li_2MnO_3 \underset{\text{heating in } O_2}{\overset{>680^\circ C \text{ in } N_2}{\rightleftharpoons}} 3\ LiMnO_2 + \frac{1}{2}O_2 \quad [7]$$

Finally, a summary of the thermal stability and decomposition reactions of $Li_4Mn_5O_{12}$ under oxygen and inert atmospheres is shown in Fig. 7.

CONCLUSION

The thermal stability and structural changes of well-crystallized $Li_4Mn_5O_{12}$ powder with a grain size of 0.1–0.3 μm under flowing O_2 or N_2 up to 930°C have been systematically investigated using TGA, XRD, and HT-XRD. In O_2, the spinel framework of $Li_4Mn_5O_{12}$ remained intact up to 750°C, but a reversible evolution/uptake of oxygen due to the reduction/oxidation $Mn^{4+} \Leftrightarrow Mn^{3+}$ was revealed with TGA as a reversible weight loss/gain upon heating/cooling the sample from 600 to 700°C and from 700 to 400°C. The sample with oxygen deficiency can be presented as $Li_4Mn_5O_{12-\delta}$ with $0 < \delta \leq 0.5$. The decomposition of $Li_4Mn_5O_{12}$ to spinel $LiMn_2O_4$ and monoclinic Li_2MnO_3

occurs at temperatures above 750°C in O_2 or air, but at 530°C in N_2. At temperatures above 680°C in N_2, both $Li_4Mn_5O_{12}$ and $LiMn_2O_4$ decompose to $LiMnO_2$ and Mn_3O_4.

ACKNOWLEDGMENT

The authors thank Dr. T. Tsunoda and Dr. M. Mukaida for helping us with the use of the SEM microscope.

REFERENCES

1. M. M. Thackeray, A. de Kock, M. H. Rossouw, D. Liles, R. Bittihn, and D. Hoge, *J. Electrochem. Soc.* **139**(2), 363 (1992).
2. M. M. Thackeray, W. I. F. David, P. G. Bruce, and J. B. Goodenough, *Mater. Res. Bull.* **18,** 461 (1983).
3. M. M. Thackeray, P. J. Johnson, L. A. de Picciotto, P. G. Bruce, and J. B. Goodenough, *Mater. Res. Bull.* **19,** 179 (1984).
4. J. M. Tarascon, E. Wang, F. K. Shokoohi, W. R. Mckinnon, and S. Colson, *J. Electrochem. Soc.* **138**(10), 2859 (1991).
5. E. Ferg, R. J. Gummow, A. de Kock, and M. M. Thackeray, *J. Electrochem. Soc.* **141**(11), L147 (1994).
6. M. M. Thackeray, A. de Kock, M. H. Rossouw, D. Liles, R. Bittihn, and D. Hoge, *in* ''Proceedings, Electrochem. Society,'' Vol. 91–3, p. 326. 1991. [Proc. Primary Secondary Lithium Batteries, 1990].
7. D. Guyomard and J. M. Tarascon, *J. Electrochem. Soc.* **140**(11), 3071 (1993).
8. D. Guyomard and J. M. Tarascon, *J. Electrochem. Soc.* **139**(4), 937 (1992).
9. R. J. Gummow, A. de Kock, and M. M. Thackeray, *Solid State Ionics* **69,** 59 (1994).
10. B. Zachau-Christiansen, K. West, T. Jacobsen, and S. Atlung, *Solid State Ionics* **40/41,** 580 (1990).
11. P. Barboux, J. M. Tarascon, and F. K. Shokoohi, *J. Solid State Chem.* **94,** 185 (1991).
12. M. M. Thackeray and M. H. Rossouw, *J. Solid State Chem.* **113,** 441 (1994).
13. J. M. Tarascon, W. R. McKinnon, F. Coowar, T. N. Bowmer, G. Amatucci, and D. Guyomard, *J. Electrochem. Soc.* **141**(6), 1421 (1994).
14. M. M. Thackeray, A. de Kock, and W. I. F. David, *Mater. Res. Bull.* **28,** 1041 (1993).
15. M. H. Rossouw, A. de Kock, L. A. de Picciotto, M. M. Thackeray, W. I. F. David, and R. M. Ibberson, *Mater. Res. Bull.* **25,** 173 (1990).
16. T. Takada, H. Hayakawa, and E. Akiba, *J. Solid State Chem.* **115,** 420 (1995).